Hindawi
International Journal of Polymer Science
Volume 2022, Article ID 4691347, 17 pages
https://doi.org/10.1155/2022/4691347

*Research Article*

# The Performance of Different $AgTiO_2$ Loading into Poly(3-Nitrothiophene) for Efficient Adsorption of Hazardous Brilliant Green and Crystal Violet Dyes

**Sara A. Alqarni**

*Department of Chemistry, College of Science, University of Jeddah, Jeddah, Saudi Arabia*

Correspondence should be addressed to Sara A. Alqarni; sasalqarni@uj.edu.sa

Received 20 October 2021; Revised 22 November 2021; Accepted 9 December 2021; Published 5 January 2022

Academic Editor: Peng He



The in-situ polymerization technology was used to successfully produce nanostructured binary nanocomposites (NCs) made from a poly (3-nitrothiophen) matrix (P3NT) that were loaded effectively with nanoparticles (NPs) of silver titanium dioxide ($AgTiO_2$), of varying percentages (10%, 20%, and 30%). A uniform coating of P3NT covers the $AgTiO_2$ NPs. Various methods were performed to confirm the fabrication of the binary P3NT/$AgTiO_2$ NCs adsorbents, such as FTIR, XRD, SEM, and EDX. Both dyes (brilliant green (B.G.) and crystal violet (C.V.)) were removed from liquid media by using the binary P3NT/$AgTiO_2$ NCs. A range of batch adsorption studies was used to optimize various factors that impact the elimination of B.G. or C.V. dyes, including the pH, weight of the binary P3NT/$AgTiO_2$ NC, proportion of $AgTiO_2$ NP, time, and temperature. The pseudo-second-order kinetics ($R^2 = 0.999$) was better adapted for the adsorption procedure's empirical data whereby the maximum adsorption capacity of the C.V. dye was 43.10 mg/g and ($R^2 = 0.996$) the maximum adsorption potential was 40.16 mg/g for B.G. dye, succeeded by the pseudo-second-order kinetics. Moreover, the adhesion of B.G. and C.V. pigments on the layers of NCs involves an endothermic reaction. In addition, the concocted adsorbent not only exhibited strong adsorption characteristics during four consecutive cycles but also possessed a higher potential for its reuse. According to the findings, the NCs might possibly be used as a robust and reusable adsorbent to remove B.G. and C.V. pigments from an aqueous medium.

## 1. Introduction

The unending discharge of pollutants in the environment has positioned water pollution amongst the few topmost environmental issues. The usage of a diversified range of dyes is characteristic of the operations of multiple industries like textile, printing, leather, petroleum, plastic, and pharmaceuticals [1]. Components of toxic organic compounds are transmitted to the wastewater during the manufacturing of colored pigments leading to the existence of numerous fragrant, polycyclic, or heterocyclic chemicals that might affect the health and well-being of humans [2]. Colorants might persist in the environment for a longer time in the form of organic molecules having a steady configuration. Alternatively, the presence of different aromatic materials of complex structures in dye wastewater tends to make the treatment of wastewater quite challenging because of its strong color efficiency stability, concentration, and inefficient degradation. As a consequence, the pretreatment of industrial wastewater containing dyes prior to disposal has grabbed increasing attention in the past few years [2]. The average annual production of 735 metric tons of dyes is done for trading purposes out of the total 10000 varieties of dyes. The available data has confirmed the discharge of more than 15% of such dyes in the form of liquid wastage in the process of commercial production [3]. The outpouring wastage from industries containing dyes is harmful to the environment that can be aligned with (i) high virulence, (ii) deficient photolytic ability, (iii) increased stability, (iv) and speedy degradation [4]. Additionally, humans also experience nausea, vomiting, and anemia due to the presence of particles of dyes in the environment [5]. In addition, the skin is allegedly exposed to heightened susceptibility and irritation after being exposed to dyes, which can potentially lead to

malignant mutation [3]. Treatment of organic pigments having a convoluted molecular composition with other compounds alters their color to poorer or brighter tones [6]. Brilliant green (B.G.) dye is a cation that has a triphenyl nitrogen structure, which is used in veterinary medicines, biopigmentation, the coloring of textiles, manufacturing of ink for colored printers, and dermatological products in the form of a supplement to chicken food for regulating the growth of parasitic organisms and fungi [7]. It tends to initiate a multitude of health issues, including cough, diarrhea, difficulty in breathing, nausea, vomiting, and painful flushes [8]. Crystal violet (C.V.) additionally recognized as methyl violet is a water-soluble dye and is classified as cationic dye triphenylmethane. It is used as a pH indicator; it is also widely used in textile industries, additives in medicine, and microbiology stain [9]. Nevertheless, C.V. dye may cause eye burn and permanent eye/cornea damage. Its inhalation gives rise to vomiting, nausea, excessive sweating, diarrhea, hypermotility, and stomachache [9]. According to Bhasikuttan et al. [10], the toxicity of C.V. dye was due to the oxidative strain produced by reactive oxygen kinds [10]. Cationic dyes are regarded as highly poisonous and dangerous in comparison to anionic dyes due to the secured binding between the positively charged atoms of cations and points of negative charges on the cellular walls. Seclusion of cationic dyes from the wastewater is hence necessary before sequestering them into water [11] which mandates the need for purification of water and elimination of dyes from the wastewater prior to its release in the water bodies. The wastewater contaminated with dyes can be treated through multiple techniques, including but not limited to coagulation, adsorption, membrane segregation, extraction of solvents, catalytic decomposition, chemical condensation, and reverse osmosis [12]. Due to the complicated aromatic structures of dyes, the standard treatment procedures fail to remove dyes from the wastewater and typically increase the stability of these dyes. The adsorption technology has lately attracted considerable attention. Due to its excellent qualities of easy operation, high effectiveness as well as the availability of different adsorbers, it is regarded as the more cheap and effective approach to remove different kinds of dyes [13]. The correlation between the columbic agents and the mounting interaction thus regulates the outstanding adsorption properties of cationic M.B. and C.V. dye. This confirms its quick attraction towards negatively charged materials [14]. In the majority of the developing nations, this approach has become popular and prospective due to its ease of operation, simplicity, lowest sludge production, and highest biosorbent regeneration rate. The financial viability of the adsorption process enables the thorough elimination of pollutants without any side effects to the environment [15]. Unluckily, the adsorption power of the majority of these adsorbents is comparatively low. Hence, adsorbents have lately been actively adapted to the surface to increase their adsorption capacity [2]. The high environmental endurance, distinctive redox electrical behavior, doped or frozen sustainability, easy synthesization, and the vast array of its uses have drawn great interest towards polythiophene (PTh) [16]. The efficiency as electrical donors, relevance as hole transmitters, thermal stability, and visible light absorption capabilities are characteristic to the controlling polymers like PTh having $\pi$-conjugated electron framework [17]. As indicated by Khatamian et al., PTh/ZnO and PTh/$TiO_2$ exhibit a higher rate of absorption of visible light and increased capacity of dye elimination as compared to pure ZnO and $TiO_2$, respectively [17]. The nitro replacement of PTh changes the polymer's electrical characteristics and hence expands its usefulness in commercial processes. PTh or replacement PTh can display strong adsorption characteristics upon coupling with either a metal or metal oxide or a mixture of both. $TiO_2$, particularly, possesses a reactive group of oxygen that engages with PTh or its by-products through a $\pi$-$\pi$ interplay occurring between the nonpolar sections of $TiO_2$ and the molecular strata of PTh [16]. In general, a diverse range of oxides including ZnO, $TiO_2$, $Bi_2O_3$, MgO, and $WO_3$ is utilized to remove numerous organic pollutants such as 17$\beta$-estradiol in their pure state or combination form with any other metal or nonmetal (carbon nanomaterials, amorphous boron, and so on) compounds [18]. $TiO_2$ has also been extensively used for preserving the environment and, particularly, photodecomposing azo pigments owing to its low cost, nontoxic properties, nonphoto corrosive, and, most of all, high dye elimination potential [19]. Nevertheless, the wide bandgap (3.2 eV) of $TiO_2$ largely limits its practical usage [20]. In addition, only ultraviolet light can stimulate $TiO_2$ for producing pairs of photoelectron holes, thus implying that the usage pace of the visible light is fairly low and the pairs of electron holes, e, and h$\mu$ are reassembled extremely quickly, mostly in nanoseconds [21]. Thus, the transformation of $TiO_2$ has become more and more interesting. Pt, Pd, and Au are the most commonly employed noble metals for $TiO_2$ modification [22]. Although expensive costs of these noble metals have pushed several researchers to use Ag as a substitute metal for improving the adsorption capacity of $TiO_2$ [19], in recent research analyses, several approaches based on the improvement of adsorbent materials in organic dye removal using Ag transformation techniques have been published. For instance, the development of surface chemistry and optimization of selective removal with the use of hydrophilic substances such as $TiO_2$ and Ag-$TiO_2$ have been propagated [23]. To the best limit of our knowledge, no studies on the adsorption comportment of $AgTiO_2$ NCs based on replaced PTh have been published in the literature to date. $AgTiO_2$ NPs aggregated with the replaced PTh matrix are inclined towards the enhancement of its ecological compatibility, prevention of gathering, minimization of susceptibility to leaching, and augmentation of adsorption capability. A novel, highly effective, and affordable, innovative adsorbent is created in this research by using an in-situ chemical polymerization technique to combine P3NT with various loads of $AgTiO_2$. This conglomerate incorporates the benefits of every component, as a result of which the adsorption efficiency of recommended adsorbents enhances because of increased active points on the backbone of the polymer string, which leads to a higher capacity of dye elimination. The XRD, FTIR, EDX, and SEM methods have been engaged for examining the structure and morphology

of NCs, whereas UV-vis spectroscopic techniques assisted in enhancing the B.G. and C.V. dye elimination capacity of the assessed NCs from the aqueous solutions. Additionally, a multitude of factors, including pH, heat, time of shaking, time, mass, and effect of ionic power, influencing the process of elimination of dyes was also examined, after which the data of adsorption was scrutinized with the help of multiple thermodynamic and kinetic criteria.

## 2. Experimental Analysis

*2.1. Reagents and Materials.* The procurement source of ethylene glycol (EG), thiophene, and ammonium persulfate (APS) was Fluka in Switzerland, whereas Sigma-Aldrich of USA was the sourcing location for dry ice, chloroform, anhydrous sodium sulfate ($Na_2SO_4$), anhydrous chloroform, chlorosulfonic acid ($HSO_3Cl$), silver nitrate, sodium hydroxide (NaOH), concentrated sulfuric acid ($H_2SO_4$), hydrochloric acid (HCl), deuterated dimethyl sulfoxide (DMSO-$d_6$, 99.8%), chlorosulfonic acid ($HSO_3Cl$), carbon tetrachloride ($CCl_4$), and nitric acid ($HNO_3$). The XFNANO Advanced Materials Supplier Inc. of China assisted in the procurement of $TiO_2$ powder. The entire range of solvents and other elements was of analytical grade and were used without being subjected to any further cleansing process. Aldrich Chemical Co. Ltd., located in Milwaukee, WC., USA, was the source of procuring a stock solution of B.G. and C.V. dyes (100 $\mu g \cdot mL^{-1}$). The extra diluted stock solutions of 5 to 25 $\mu g \cdot mL^{-1}$ were prepared with the aid of deionized water. The range of Bitton-Robinson (BR) buffers of pH values ranging from 2 to 11 in conjunction with HCl and/or NaOH (0.1 $mol \cdot L^{-1}$) has been used as extractive agents for the sorption of dyes (binary P3NT/30%$AgTiO_2$ NCs).

*2.2. Apparatus.* Ultrasonication was achieved with a 360 W, 40 kHz, model number GD0610, Guangdong, China. Bruker model D8, in assistance with Cu Ka irradiations, served as the basis for performing powder X-ray diffraction (XRD) analysis. The use of a Model Quanta 250 FEG yielded the scanning electron microscopy (SEM) images. The acquisition of $^1$HNMR spectra on the Brucker DPX 600 MHz spectrometer's DMSO-$d_6$ with the use of intrinsic standard tetramethylsilane (TMS) was done at normal room temperature settings. A JASCO model spectrometer was used for attaining the Fourier transform Infrared (FTIR) spectrum in the band of 4000–300 $cm^{-1}$. The UV-apparent spectrophotometer (190–1100 nm) (model Lambda 25, PerkinElmer, USA) having a wide pathway of 10 mm quartz cell was used to determine all the spectrophotometric dimensions, thus proving the elimination of B.G. and C.V. dyes by engaging (binary P3NT/30%$AgTiO_2$ NCs) absorbents. A digitized micropipette (Volac) was used for the preparation of the stock solutions, whose pH determination was done by using a pH meter (Orion/model EA 940). A four-decimal number digital balance (Citizen Scales Inc., USA) of high sensitivity was also used in the study. The Milli-Q Plus tool (Millipore, Bedford, MA, USA) assisted in obtaining deionized water that was mixed with produced solutions.

*2.3. Preparation of 3-Nitrothiophene (3NT).* Blatp et al. employed the technique illustrated in scheme 1 for preparing 3-NT for the first time ever [24]. A 200 mL beaker was used to mix 13 mL anhydrous chloroform and 25 g of $HSO_3Cl$, followed by mechanical stirring and the addition of 7 mL thiophene for a time of 4 minutes. Dry ice was added directly to this mixture to maintain its temperature at zero degrees. Then, the reaction mix was brought back to room temperature, after which dry ice was again added to it for decomposition of surplus $HSO_3Cl$. The layers of the resultant mix were segregated, out of which the aqueous layer was taken out by using 10 mL chloroform. The mixed coatings of chloroform were rinsed with 15 mL water and distilled after dehydrating with anhydrous $Na_2SO_4$. 10 g thiophene-2-sulfonyl chloride was extracted after six similar rounds, which undergoes solidification after cooling down. 10 g of thiophene-2-sulfonyl chloride was poured drop by drop in the time of an hour into a 50 mL boiling solution of $HNO_3$ with an automatic stirring kept between 25 and 30°in a cold-water bath. This mixture was kept at 40° for an hour before being poured on ice; as a result of which, the organic material was segregated by using 70 mL $CCl_4$, which was rinsed with water, distilled, and dried. As a result, 10 g of thiophene-2-sulfonyl chloride yielded 8 g of 4-nitrothiophene-2-sulfonyl chloride fuming at 145–150°/4 mm, along with 2 g of 5-nitrophene-2-sulfonyl chloride boiling at 133–136°/4 min. A mixture of 30 mL water and 8 g of 4-nitrothiophene-2-sulfonyl chloride was boiled for 4 hours under reflux so that all the elements of acid chloride were disintegrated. The resultant transparent yellow solution was kept for the whole night, after which 70 mL concentrated $H_2SO_4$ and 50 g of ice were added to it. The eventual solution was subjected to heating at 140°C until the extremely heated steam was released, and it was maintained at this temperature to perform the process of distillation. All the proportions of the reaction mix needed a span of 90 minutes to be fully distilled. The weight of 3NT resulting in distillate after precipitation was 3 g.

*2.4. Preparation of P3NT.* The in situ polymerization technique was used for preparing pure P3NT [25]. The standard method of preparation includes the following steps: a mixture of 2 mL of the 3NT and 100 mL of 1 M HCl is poured in a three-neck flask of 250 mL volume. After ultrasonication of this mixture for a span of 30 minutes, it was left to cool down in an ice bath until it reached the temperature of 0–4°C and was consistently stirred till then. In about 30 minutes, drops of 3 g of a cooled down solution of ammonium persulfate (APS) diluted in 100 mL of 1 M HCl were added to the prepared solution under the atmosphere of nitrogen and was stirred continually at 0–4°C. In the nitrogen environment, the polymerization process has been sustained with continuous mixing at 0–4°C for 24 hours. The resultant precipitate was accumulated by ultracentrifugation before being rinsed off with deionized water multiple times until the filtrate turns colorless and the final black powdery substance is dehydrated at 50°C for a time of 12 hours.

*2.5. Preparation of $AgTiO_2$ NPs.* The $TiO_2$ powders (0.005 wt%) were first dehydrated in the oven for 3 hours'

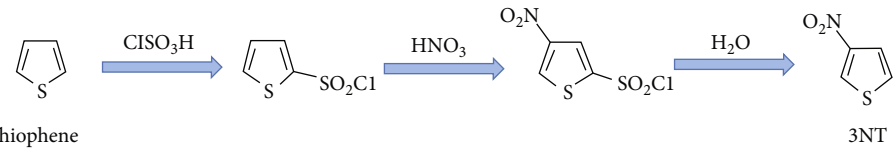


Scheme 1: Synthesis of 3-nitrothiophene.

time followed by its immediate mixing with 20 mL solution made by blending deionized water and EG in the ratio of 1 : 4 along with 0.01 wt% of NaOH, which was the restricted quantity for the surface synthesis of Ag particles in $TiO_2$. After this step, the mix was turned wet by a magnetic stirrer for 24 hours, and then, it was dispersed for 3 minutes with the ultrasonic probe at the frequency of 23 kHz and 500 W power. Under generic conditions, $AgNO_3$ ($3.47 \times 10^{-4}$ M) was mixed with the resultant $TiO_2$ solution after dispersion that was amalgamated at 25°C for 15 minutes with the aid of the sonochemical method.

*2.6. Preparation of P3NT/AgTiO$_2$ NCs.* Initially, 10% $AgTiO_2$ NPs were poured into a three-collared flask of 250 mL volume that already contained 100 mL of 1 M HCl, after which an ultrasonic machine aided to blend the mixture at room temperature for 2 hours. Then, 2 mL of 3NT was added to this mixture, followed by its ultrasonication for 30 minutes. This mixed solution was subjected to an ice bath for cooling down till it reached 0–4°C and was continually stirred till then. 3 g solution of ammonium persulfate (APS), which was already cooled down and diffused in 100 mL of 1 M HCl, was poured under the nitrogen environment drop by drop to the above-made solution in a span of 30 minutes and was constantly stirred at 0–4°C. The ultracentrifugation method assisted in the collection of precipitate, which was cleaned with deionized water repeatedly until attaining the colorless filtrate. The resultant fine black powder was dehydrated at 50°C for a time of 12 hours. Scheme 2 depicts the route of synthesis of P3NT/$AgTiO_2$ NCs. This analysis was repeated twice with 20% and 30% proportions of $AgTiO_2$. Table 1 depicts the recommended abbreviations of P3NT/$AgTiO_2$ NCs.

*2.7. Batch Extraction Step.* A unique weight ($0.005 \pm 0.002$ g) of the binary P3NT/30%$AgTiO_2$ NCs was balanced at pH 8 with 50 mL solvent comprising C.V. dye (5 mg·L$^{-1}$). Another weight ($0.005 \pm 0.002$ g) of solid-phased binary P3NT/30%$AgTiO_2$ NCs was balanced at pH 6 with 50 mL solvent comprising B.G. dye (5 mg·L$^{-1}$). A shaker was used for stirring the experimental solutions for 75 minutes. The photometric examination of the blank reagents [3] was used to estimate the remaining dyes after the separation of the aqueous solutions. The quantity of adsorbed dyes on P3NT/30%$AgTiO_2$ NCs was then estimated by calculating the differences in the rate of absorption of dyes in the aqueous media pre- (Ab) and postremoval dyes (Af). Eventually, the adsorption ratio (%$E$), (equation (2)) the entire quantity of dyes secured after equilibration of per unit ($q_e$), and the dispersion coefficient ($K_d$) of the adsorbed dyes on binary P3NT/30%$AgTiO_2$ NCs (equation (3)) were computed. The adsorption ratio and distribution coefficient are calculated by averaging a trio of independent measurements, and mostly, ±2% precision was derived. Following this, additional analysis was carried out on the effect of the temperature and time of stirring on the binary P3NT/30%$AgTiO_2$ NCs' dye retention capacity.

$$\text{Adsorption}(\%) = \frac{C_0 - C_t}{C_0} \times 100(\%),$$
$$q_t = \frac{(C_0 - C_t)V}{m}, \quad (1)$$

where $C_0$ and $C_t$ are the initial and final concentrations of dyes in solution (mg/L), respectively, $V$ is the volume of the solution (L), and $m$ is the mass of the P3NT/30%$AgTiO_2$ NCs used (g).

*2.8. Environmental Applications and Sample Collection.* Water samples were gathered from three variable sources to investigate the dye removal potential of the binary P3NT/30%$AgTiO_2$ NC adsorbents: (I) water of the Red Sea flowing in front of Jeddah city, KSA, (II) tap water of the chemistry department labs located in the University of Jeddah, Jeddah city, KSA, and (III) sample of wastewater collected from wastewater treatment plants located at King Abdulaziz University, Jeddah city, KSA. The samples were collected by using a 0.45 $\mu$m membranous filter and were secured at 5°C in dark Teflon bottles. 100 mL samples were apportioned and held at pH 6 for B.G. dye and pH 8 for C.V. dye, respectively. Consequently, these dye solutions were traversed through binary P3NT/30%$AgTiO_2$ NC adsorbents in the solid phase, after which the resultant dyes' concentration was calculated through a spectrophotometer.

## 3. Results and Discussions

### 3.1. Characterization of Samples

*3.1.1. $^1$HNMR and FT-IR Studies.* $^1$H NMR in DMSO-D6 (Figure S1) was the first to examine the chemical composition of the produced 3NT. $^1$H NMR indicated the group of nitrogen on the aroma-rich ring by presenting a strongly descending singlet peak at $\delta$-8.8 (b) correspondent to the fragrant proton (Hc) ortho position of two extremely electron-pulling sulfonyl and nitro groups. The existence of the nitro group on the aromatic band caused the displacement of the $\delta$ value that associates with several extra peaks in the spectra.

The FTIR spectrum of P3NT, $AgTiO_2$ NPs, binary P3NT/10%$AgTiO_2$ NCs, binary P3NT/20%$AgTiO_2$ NCs, and binary P3NT/30%$AgTiO_2$ NCs. has been represented

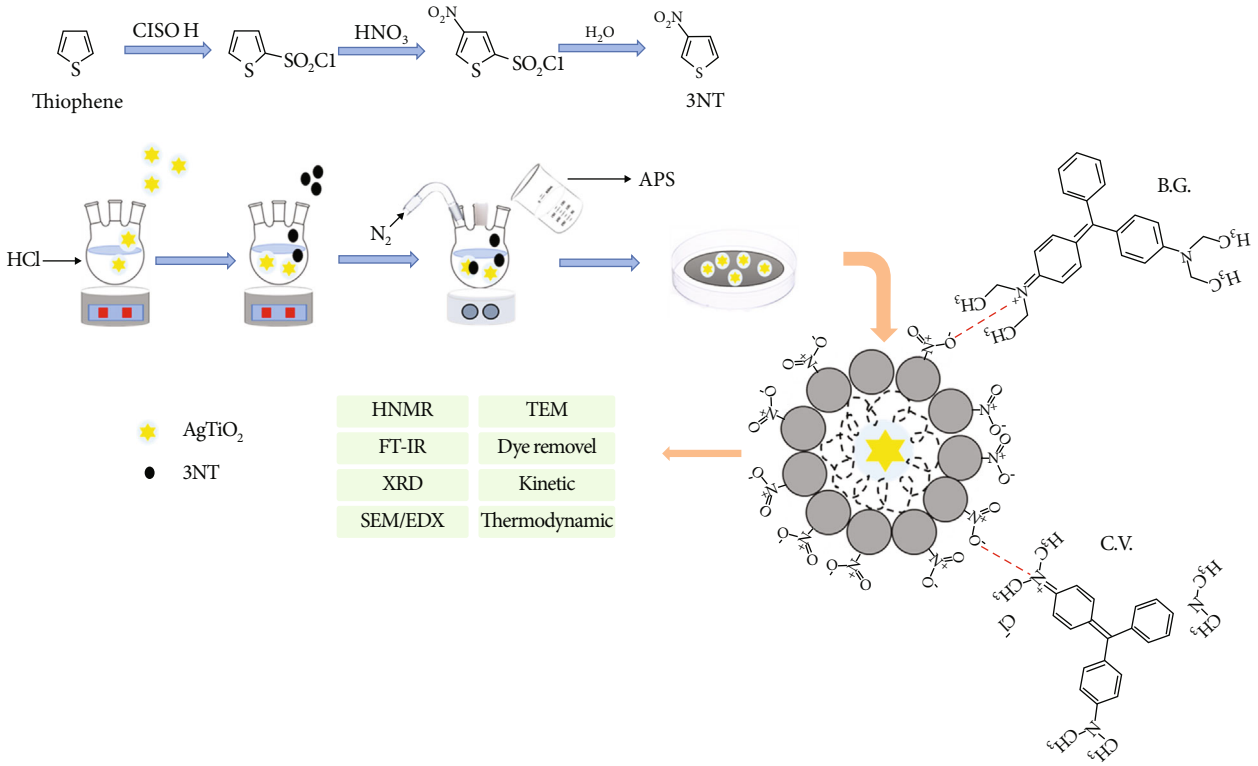


Scheme 2: Illustration of the preparation of the binary P3NT/$AgTiO_2$ NCs and adsorption of B.G. and C.V. dyes on the binary P3NT/$AgTiO_2$ NCs.

Table 1: The chemical compositions for P3NT/$AgTiO_2$ NCs.

| Nanocomposites | 3NT (weight, g) | $AgTiO_2$ (weight, g), (%) |
|---|---|---|
| P3NT | 2 | 0 |
| Binary P3NT/ 10%$AgTiO_2$ NCs | 1.8 | 0.2 (10%) |
| Binary P3NT/ 20%$AgTiO_2$ NCs | 1.6 | 0.4 (20%) |
| Binary P3NT/ 30%$AgTiO_2$ NCs | 1.4 | 0.6 (30%) |

in Figure 1. According to Figure 1(a), the P3NT produced herein depicts bands ranging between 2800 and 3500 $cm^{-1}$ because of the stretching vibration [26]. On the other hand, the bands at 1462 $cm^{-1}$ are visible because of symmetric C=C stretching vibration and those at 1709 $cm^{-1}$ are visible due to asymmetric C=C stretching vibration[27]. The abrupt band appearance at 783 $cm^{-1}$ is equivalent to the out-of-plane vibrational mode of the bond shared between C and H in the thiophene ring [27]. An in-plane deformity in the C-H bond is signified by an apparent vibrational band observed at 1042 $cm^{-1}$ [28]. Alternatively, the emergence of a band at 692 $cm^{-1}$ matching the bending mode of the C-S bond proves the existence of thiophene [29]. Asymmetrical stretching of $NO_2$ (N-O) can be seen at 1542 $cm^{-1}$, and the $NO_2$'s symmetrical (N-O) stretching maxima appear at 1336 $cm^{-1}$. The band apparent at 817 $cm^{-1}$ is believed to have dynamic C-N stretching vibrational attributes [30]. P3NT formation is confirmed through this result. The binary scales of NCs shown in Figures 1(b)–1(e) are present in all three spectra at the typical bands at about 700 $cm^{-1}$ designated for $TiO_2$ [31]. Furthermore, the production of binary NCs, as well as the interaction amongst the polymer chain and $AgTiO_2$ NPs, is largely confirmed by all bands similar to P3NT. The alteration in the position of the P3NT band (from 1462 to 1450 $cm^{-1}$ and from 1709 shifted to 1654 $cm^{-1}$) along with that of N-O (1336 shifting to 1339 $cm^{-1}$ and 1542 shifting to 1547 $cm^{-1}$) and a small decrease of band amplitude indicates that NCs were developed successfully.

*3.1.2. XRD Studies.* Figure 2 displays the XRD patterns of P3NT, of $AgTiO_2$ NPs, of the binary P3NT/10%$AgTiO_2$ NCs, of the binary NCs of P3NT/20%$AgTiO_2$, and of the binary NCs of P3NT/30%$AgTiO_2$. In P3NT, the amorphous character of the polymer is defined by a broad diffraction peak visible within a range of $2\theta$ values falling between 15° and 30° [32]. The apparent nano-Ag crests at $2\theta$ values linked with 38.45°, 46.35°, 64.75°, and 78.05° corresponding to the respective levels of [1 1 1], [2 0 0], [2 2 0], and [3 1 1] authenticate the existence of $AgTiO_2$ NPs in the binary P3NT/10%$AgTiO_2$ NCs, P3NT/20%$AgTiO_2$ NCs, and P3NT/30%$AgTiO_2$ NCs jointly [33]. $TiO_2$ analysis led to $2\theta$ value peaks of 25.22°, 37.78°, 47.94°, 54.15°, 54.96°, and 62.69° that were arranged at respective [101], [004], [200], [211], [105], and [204] levels of $TiO_2$ in a typical pattern characteristic to the anatase phase (JCPDS card no. 01-086-1157) [34]. The presence of $AgTiO_2$ NPs in all the

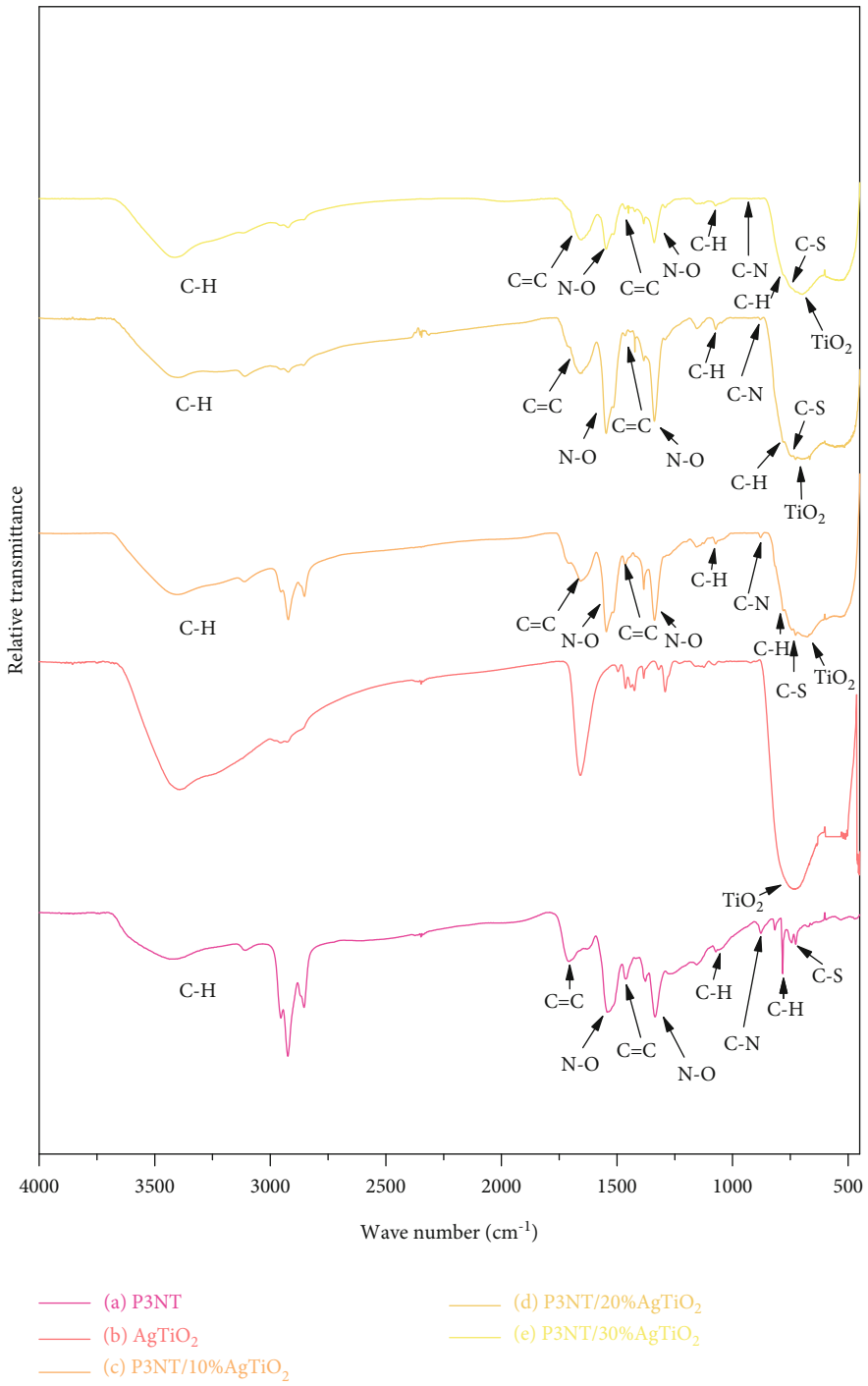


Figure 1: FTIR of P3NT (a), $AgTiO_2$ NPs (b), binary P3NT/10%$AgTiO_2$ NCs (c), binary P3NT/20%$AgTiO_2$ NCs (d), and binary P3NT/30%$AgTiO_2$ NCs (e).

binary NCs is pointed out by the emergence of $AgTiO_2$ crests. P3NT's typical peak intensity is small in the case of binary NCs, which points towards the complete absorption of P3NT on the surface of $AgTiO_2$ NPs. This finding may also indicate strong adhesiveness between the surfaces of P3NT and $AgTiO_2$ NPs. Meanwhile, the strength of the distinctive diffractor peaks of the pure $AgTiO_2$ was higher as compared to that of the $AgTiO_2$ peaks in the NCs, which indicates the impact of the P3NT covering layer on $AgTiO_2$'s crystalline structure. Thus, the observations of FTIR and XRD tests demonstrate the binary NCs being successfully produced, depicting excellent crystallinity and capability of interacting chemically.

*3.1.3. SEM and EDX Studies.* The P3NT surface morphology and its composites at varying loads of $AgTiO_2$, as shown in

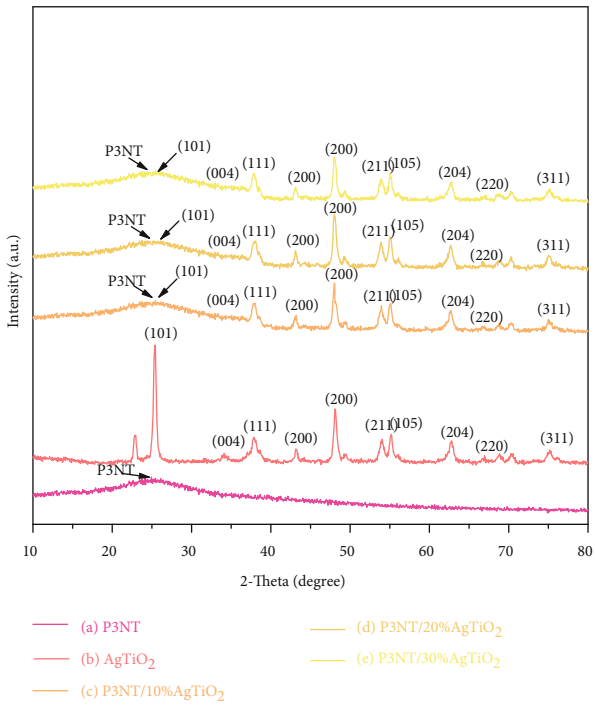


FIGURE 2: XRD pattern of the P3NT (a), $AgTiO_2$ NPs (b), binary P3NT/10%$AgTiO_2$ NCs (c), binary P3NT/20%$AgTiO_2$ NCs (d), and binary P3NT/30%$AgTiO_2$ NCs (e).

Figure 3, were examined to assess the surface characteristics of the manufactured NCs. Figure 3(a) depicts the SEM image of P3NT, which reflects the irregularity of the polymer's morphology. The roughly homogeneous spherical form of $AgTiO_2$ NPs is exhibited in Figure 3(b). In comparison to the pure $AgTiO_2$ NPs, the variable morphologies of the binary P3NT/10%$AgTiO_2$ NCs, the binary P3NT/20%$AgTiO_2$ NCs, and the binary P3NT/30%$AgTiO_2$ NCs are represented in Figures 3(c), 3(d), and 3(e), respectively. The $AgTiO_2$ NP surface is covered by layers of P3NT in case of binary P3NT/10%$AgTiO_2$ NCs, appearing in the form of tiny, assembled droplets of identical diameter with uneven absorbent edges that are favorable for the adsorption process. The increase in $AgTiO_2$ NP ratio causes enhancement of absorbent points on the surfaces of NCs as exhibited by the binary P3NT/20%$AgTiO_2$ NCs and the binary P3NT/30%$AgTiO_2$ NCs, wherein the binary P3NT/30%$AgTiO_2$ NCs apparently have a large number of porous locations that trap the dyes for being adsorbed on that surface. The binary P3NT/$AgTiO_2$ NC surfaces exhibit the possibility of adsorption of B.G. and C.V. dyes as concluded in Figure 3. Moreover, the existence of S, C, N, and O in P3NT and maxima of diffraction of Ag, Ti, and O are exhibited by the EDX spectrum of P3NT/30%$AgTiO_2$ NCs as shown in Figure 4, which demonstrates that the elements in the NC matrix are homogeneously distributed and further proves the prevalence of $AgTiO_2$ and P3NT in NCs.

*3.2. Removal of C.V. and B.G. Dyes.* P3NT, binary P3NT/10%$AgTiO_2$ NCs, binary P3NT/20%$AgTiO_2$ NCs, and binary P3NT/30%$AgTiO_2$ NCs were developed and symbolized for further application in B.G. and C.V. dye removal processes from the aqueous phase. Figure 5 showed B.G. and C.V. dyes' removal proportion of P3NT, binary P3NT/10%$AgTiO_2$ NCs, binary P3NT/20%$AgTiO_2$ NCs, and binary P3NT/30%$AgTiO_2$ NCs. The findings confirmed higher dye removal potential of binary P3NT/30%$AgTiO_2$ NCs in comparison to others. Hence, this has been chosen for studying and comparing the dye removal capacity for two distinct dyes, namely, B.G. and C.V.

The electronic spectra of C.V. and B.G. dyes obtained from the aqueous solution phase demonstrated a peak of absorption at $690 \pm 2$ nm for C.V. and $627 \pm 2$ nm for B.G. pigments, although the peak values dropped substantially following its stirring with the binary P3NT/30%$AgTiO_2$ NCs in the solid phase as represented in Figure 6. This action confirms the dye removal efficacy of binary P3NT/30%$AgTiO_2$ NCs from the aqueous media.

### *3.3. Retention Profile of C.V. and B.G. Dyes from the Aqueous Solution to the Binary P3NT/30%$AgTiO_2$ NCs*

*3.3.1. Influence of pH on Adsorption.* The pH of the solution is one of the key criteria for getting dyes' adsorption. Critical examination of the sorption profile was done post stirring the aqueous media containing C.V. and B.G. dyes at various pH levels with the solid-phase NCs of binary P3NT/30%$AgTiO_2$ for a span of 75 minutes at room temperature. All dyes in the liquid phase were determined photometrically post attaining the equilibrium [3]. However, the rise in pH level increases the percentage of sorption (%E) of C.V. sorption on the surface of binary P3NT/30%$AgTiO_2$ NCs until pH reaches the value of 8. However, after this level, the increased pH causes a decrease in the percentage of sorption. Likewise, the %*E* of B.G. sorption on the binary P3NT/30%$AgTiO_2$ NCs grows distinctly with the rising level of pH till the value of 6, after which the increase in pH level decreases the percentage of sorption. Characteristic data has been depicted in Figure 7. Hence, according to this study, the best value for C.V. and the optimal value for B.G. are pH = 8 and pH = 6, respectively, after being subjected to modification by NaOH and/or HCl.

*3.3.2. Effect of Mass on Adsorption.* The impact of the mass of the solid-phase binary P3NT/30%$AgTiO_2$ NCs on the proportion of dye adsorption from aqueous media was extracted for this study based on C.V. and B.G. dyes at a 5 mg/L concentration level as shown in Figure 8, which exhibits an increase in the percentage of dyes eliminated from the aqueous media from 81.6% to 98.1% with an alteration of the dose of binary P3NT/30%$AgTiO_2$ NCs from 5 mg to 20 mg considering the B.G. dye. Contrastingly, an increase of dye removal efficiency was seen from 75.8 to 98.7% by raising the dose of binary P3NT/30%$AgTiO_2$ NCs for B.G. dyes from 5 mg to 20 mg. Such spikes in the dye removal efficiency can be attributed to the availability of a greater potential number of active sites for adsorption due to the increased quantity of the solid phase. Thus, in this study, 5 mg of binary P3NT/30%$AgTiO_2$ NCs corresponding to 78% for C.V. and 72% for B.G. was engaged

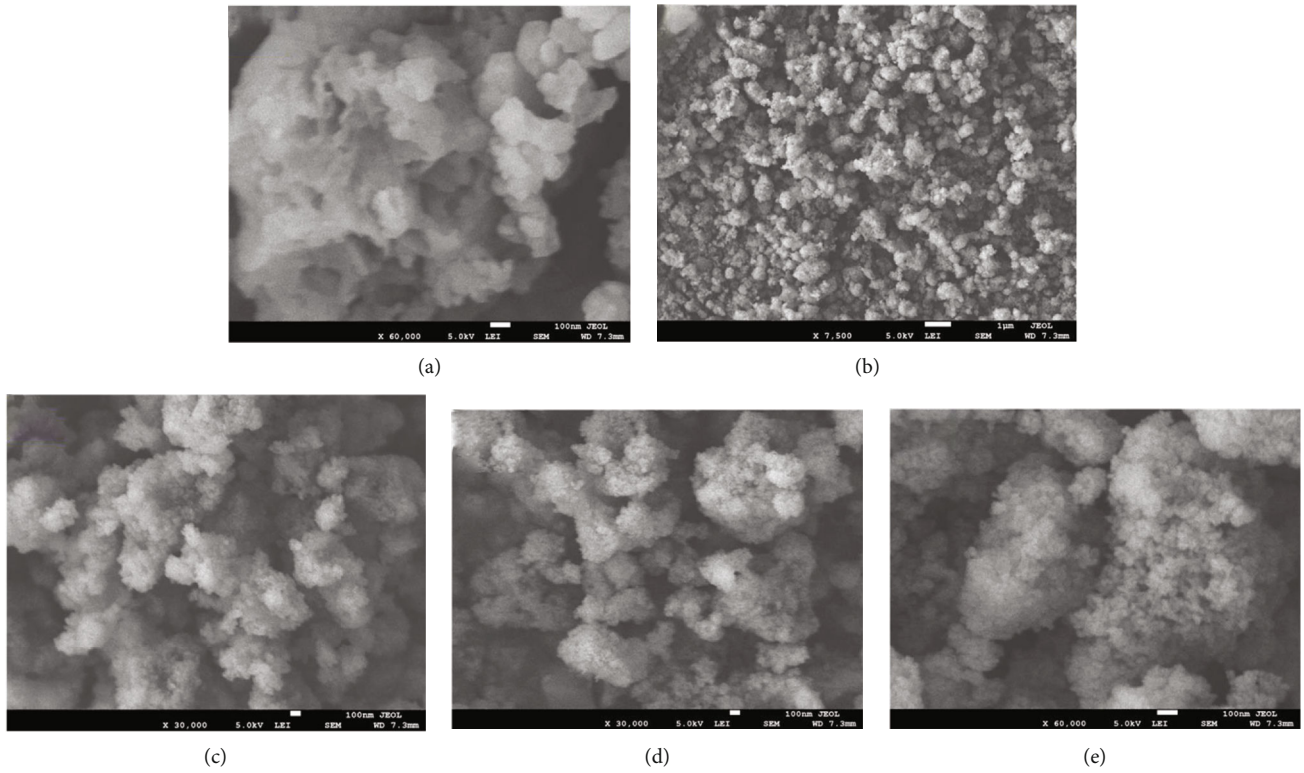


Figure 3: SEM images of the P3NT (a), $AgTiO_2$ NPs (b), binary P3NT/10%$AgTiO_2$ NCs (c), binary P3NT/20%$AgTiO_2$ NCs (d), and binary P3NT/30%$AgTiO_2$ NCs (e).

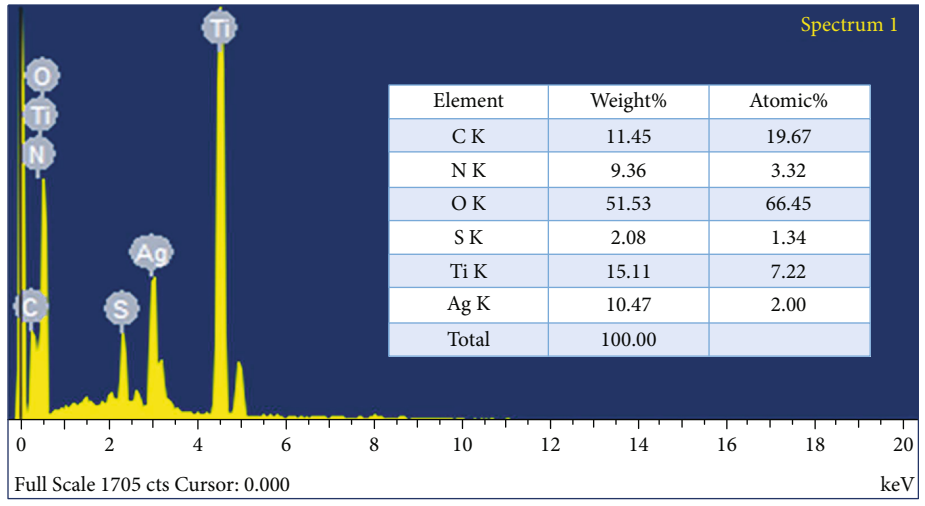


Figure 4: EDX analyses of the binary P3NT/30%$AgTiO_2$ NCs.

for analyzing the impact of additional parameters on the process of adsorption.

*3.3.3. Effect of Time and Temperature.* This research studied the effect of contact time on dye removal by the binary P3NT/30%$AgTiO_2$ NCs adsorbent; the results of which are displayed in (Figure 9). The investigation showed that the adsorption process and the increment in contact time were directly related to each other. Areas depicting a higher amount of dye adsorption in the initial 50 minutes exhibited the attainment of equilibrium of B.G. and C.V. dye removal rates within a span of 75 minutes. A couple of steps of the dye absorption process in the binary P3NT/30%$AgTiO_2$ NCs have been proposed by this finding as mentioned below: (1) a quick B.G. and C.V dye transfer to the external surface of the binary P3NT/30%$AgTiO_2$ NCs and (2) a significantly delayed dye propagation between the bundles of the binary P3NT/30%$AgTiO_2$ NCs. In addition, this study evaluated the effect of temperatures of aqueous media on the adsorption procedures of B.G. and C.V. dyes. The samples were tested at 4 different temperature ranges, including 283, 295, 313, and 328 K, with continual stirring. The results

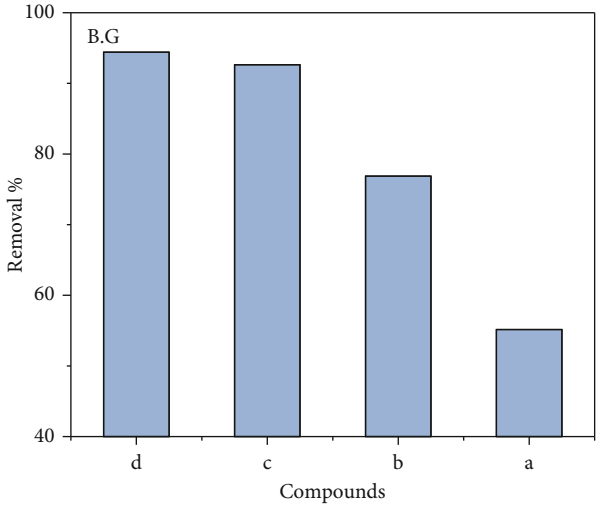


(a) P3NT
(b) binary P3NT/10%$AgTiO_2$(1) NCs
(c) binary P3NT/20%$AgTiO_2$(2) NCs
(d) binary P3NT/30%$AgTiO_2$(3) NCs

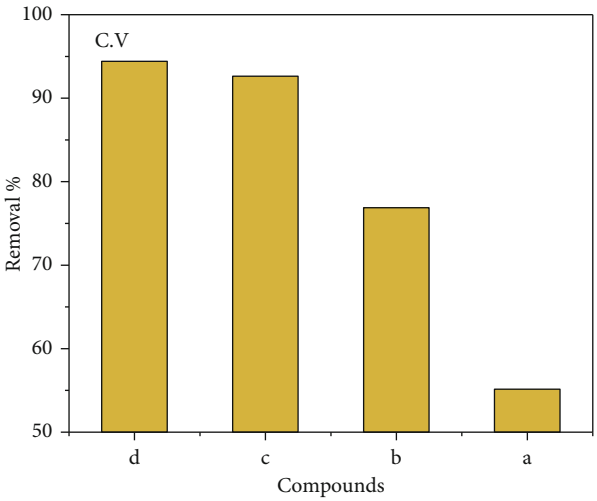


(a) P3NT
(b) binary P3NT/10%$AgTiO_2$(1) NCs
(c) binary P3NT/20%$AgTiO_2$(2) NCs
(d) binary P3NT/30%$AgTiO_2$(3) NCs

Figure 5: Removal efficiency of P3NT (a), binary P3NT/10%$AgTiO_2$ NCs (b), binary P3NT/20%$AgTiO_2$ NCs (c), and binary P3NT/30%$AgTiO_2$ NCs (d) of B.G. and C.V. dyes.

indicated that a significant elevation in the solution's temperature resulted in the associated increased dye removal by the binary P3NT/30%AgTiO2 NCs, as depicted in Figure 10. As proposed in conclusion, the endothermic nature of the adsorption process is suggested.

*3.3.4. Effect of Ionic Strength.* $KNO_3$ represents the impact of ionic power, which creates multiple states of adsorption that accords the status of being attractive or repulsive to the dye

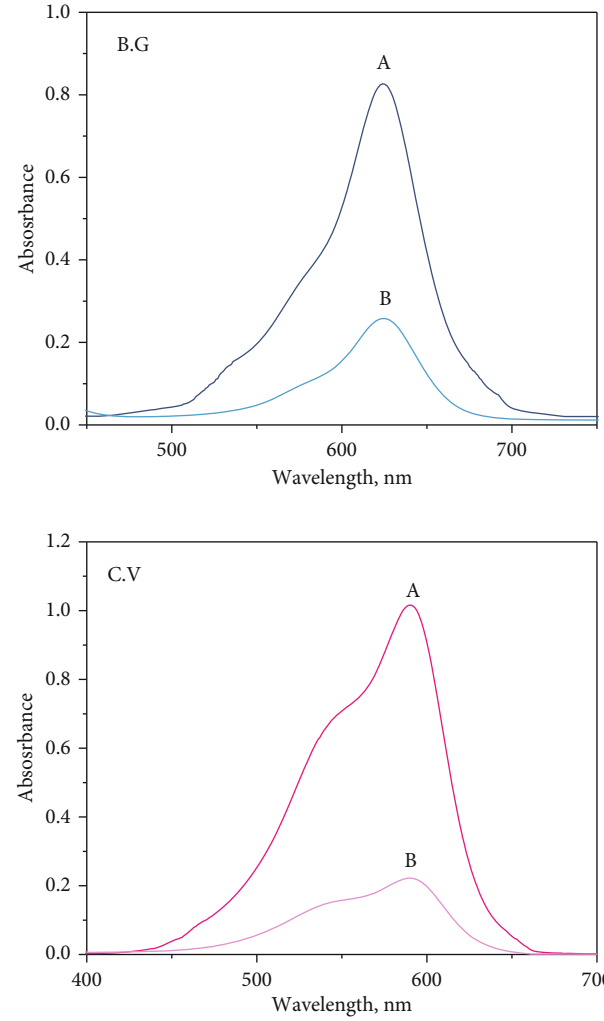


Figure 6: The electronic spectrum of B.G. dye and C.V. dye in the aqueous phase in the absence of solid phase (a) and after adding solid-phase binary P3NT/30%$AgTiO_2$ NCs and stirring for 75 mins (b).

species as well as surfaces of solid phases, known as electrostatic interactions. This study investigates the impact of ionic strength ($KNO_3$) on the adsorption power of B.G. and C.V. dyes in the solid-phased binary P3NT/30%$AgTiO_2$ NCs. A variety of concentrations of ionic strength ($KNO_3$), such as 0.025, 0.05, 0.075, and 0.1 mol/L, was used to process the adsorption experiments, as displayed in Figure 11. The results show that an increase in the ionic solution leads to a slight decline in the adsorption rate of B.G. and C.V. dyes. This reduction can be attributed to the accumulation of the charge load near the adsorbent surface species eliminated by binary P3NT/30%$AgTiO_2$ NCs. The presence of cations like $K^+$ reduces the interplay between the adsorbent surface and dye species [35].

*3.4. Kinetic Behavior of B.G. and C.V. Dye Sorption in the Binary P3NT/30%$AgTiO_2$ NC Solid Phase.* The examination of the kinetic reactivity of dyes from the aqueous media to the solid-phase binary P3NT/30%$AgTiO_2$ NC adsorbent is

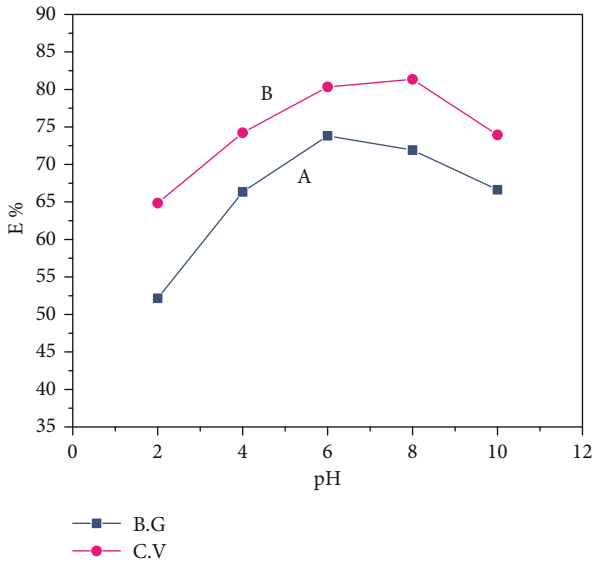


Figure 7: Impact of the solution's pH on the sorption percentage of B.G. (a) and C.V. (b) dyes from aqueous solutions onto (0.005 ± 0.002 g) the binary P3NT/30%$AgTiO_2$ NCs with 75 min of stirring at 22 ± 0.1°C.

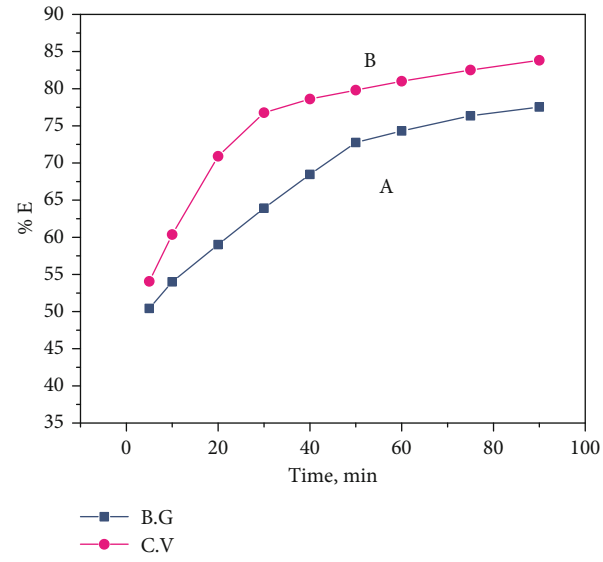


Figure 9: Impact of stirring time on the sorption percentage of dye species B.G. (a) and C.V. (b) from aqueous solutions to the binary P3NT/30%$AgTiO_2$ NCs at 22°C temperature.

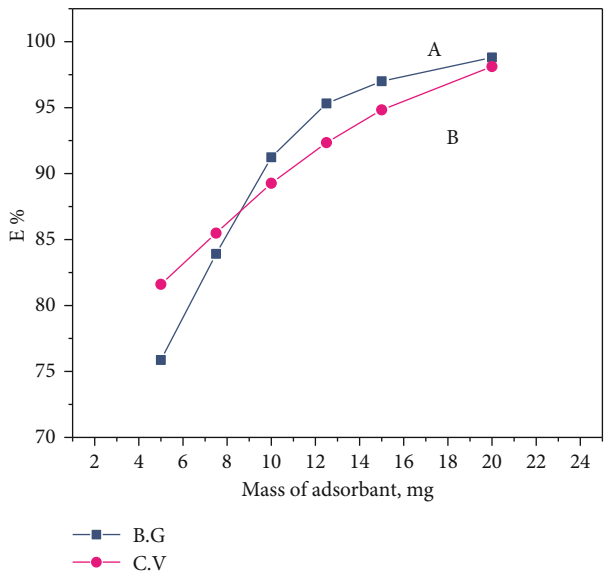


Figure 8: Impact of mass of the binary P3NT/30%$AgTiO_2$ NCs on the adsorption percentage of dye species B.G. (a) and C.V. (b) from aqueous media with stirring time of 75 minutes at 22°C temperature settings.

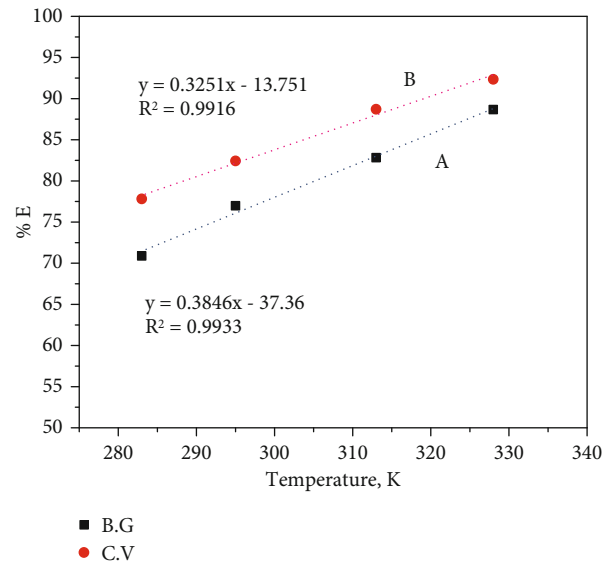


Figure 10: Impact of temperature on the sorption percentage of B.G (a) and C.V (b) dyes from aqueous solutions to the surface of binary P3NT/30%$AgTiO_2$ NCs at 283 K, 295 K, 313 K, and 328 K.

very crucial. It offers a significant understanding of the mechanisms of adsorption and reactions for sorption stages. The adsorption depends on the diffusing rate between the particles and the total transport rate, as well as the rate of film diffusion, affecting the number of dyes held by the solid phase of binary P3NT/30%$AgTiO_2$ NCs. After assessing the mixing time of the dyes, the consequential inferences were engaged for defining the dyes' adsorption procedure's half-life time ($t_{1/2}$) from the aqueous solutions to the adsorbent of binary P3NT/30%$AgTiO_2$ NCs, wherein both these were mutual providers. The log $C/C_0$ versus time plots were done to establish the $t_{1/2}$ of the binary P3NT/30%$AgTiO_2$ NCs for adsorption of B.G. and C.V. dyes. The $t_{1/2}$ value was chosen to be 1.73 ± 0.05 min for B.G., along with the dye value for C.V. 1.73 ± 0.05 min [3], in accordance with $t_{1/2}$ values, as stated before. The species of adsorbed dyes on the adsorbents of binary P3NT/30%$AgTiO_2$ NCs was in line with the Weber–Morris model [3]:

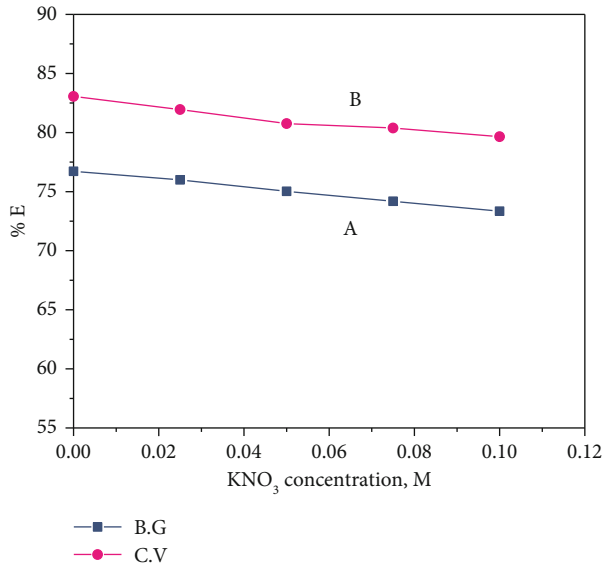


Figure 11: Impact of concentration of $KNO_3$ on the adsorption percentage of B.G. (a) and C.V. (b) dyes from the aqueous phase onto the binary P3NT/30%$AgTiO_2$ NCs at 22°C temperature.

$$q_t = R_d(t)^{1/2}. \quad (2)$$

$R_d$ implies the rate constant of transmission of dyes between the particles, and $q_t$ is the concentration of adsorbed dyes at time $t$. The graph of $q_t$ against time is depicted in Figure 12. $R_d$'s numbers extracted from Weber's two particular slopes–Morris plots are visible (Figure 12). For the B.G. dye, $R_d$ equals 2.05 mg·g$^{-1}$, where correlation coefficient $R^2 = 0.985$, and for C.V. dye, $R_d$ equals 2.19 mg·g$^{-1}$ was obtained with the correlation coefficient $R^2 = 0.926$. The following equation displays the kinetic equation of the function of fractional power, which may be modified in accordance with the Freundlich equation as follows [36]:

$$\ln q_t = \ln a + b \ln t, \quad (3)$$

where $t.q_t$ (mg/g) is the quantification of dye species adsorbed per unit mass of the binary P3NT/30%$AgTiO_2$ NCs and, simultaneously, $a$ and $b$ are coefficients with $b < 1$, using the equation of fractional power function to the experimental information of the adsorption method. Figure 13 reveals that the information is in agreement with the correlation coefficient ($R^2$) values of 0.967 and 0.977 for the B.G. and C.V. dyes, respectively. The values of $a$ and $b$ are displayed in Table 2, and the conclusion of the data received is that for describing the adsorption of dye species by the binary P3NT/30%$AgTiO_2$ NCs, and the fractional power function kinetic model is ruled out due to its complexity.

Lagergren's equation is also a prominent formula used to evaluate the liquid-phase systems' adsorption rate. In this study, the difference in the rate of adsorption from aqueous media to the solid-phase binary P3NT/30%$AgTiO_2$ NC

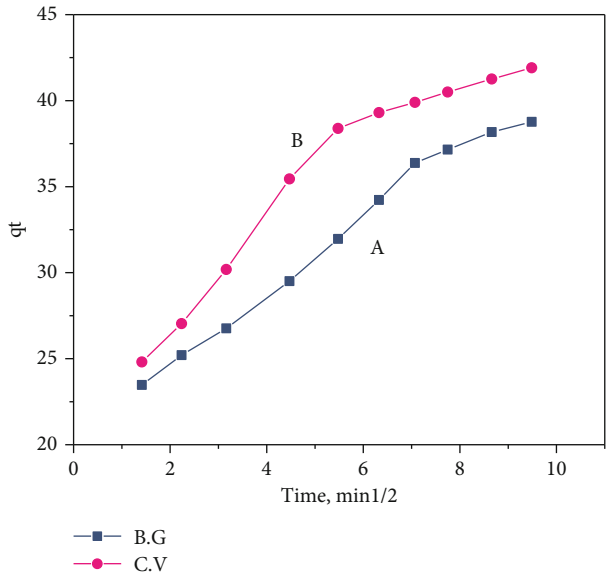


Figure 12: Weber–Morris scheme of the sorbed B.G. and C.V. dyes from aqueous solutions to the binary P3NT/30%$AgTiO_2$ NCs versus the square root of time. Experimental conditions are expressed in the batch extraction step.

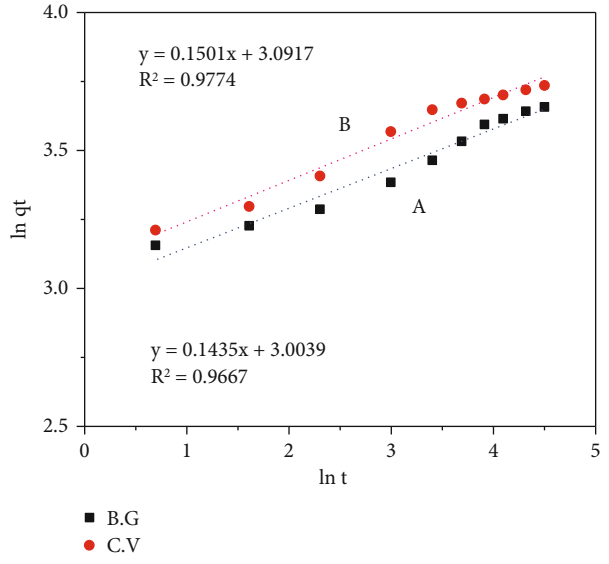


Figure 13: Fractional power model designs of B.G. and C.V. dyes from aqueous solutions to the binary P3NT/30%$AgTiO_2$ NCs. Experimental conditions are illustrated in the batch extraction step.

adsorbent depending upon the type of dyes (B.G. and C.V.) was computed with the help of Lagergren's equation [37]:

$$\log (q_e - q_t) = \frac{\log q_e - K_{\text{Lager}} t}{2.303}, \quad (4)$$

where $q_e$ implies the overall range of various types of dyes adsorbed at equilibrium per unit mass of sorbent, $K_{\text{Lager}}$ reflects the first-order total rate constant for the retention procedure, and $t$ stands for time. The $\log (q_e - q_t)$ versus

Table 2: Criteria of multiple kinetic models for B.G. and C.V. dyes' adsorption on the surface of binary P3NT/30%AgTiO2 NCs at 295 K.

(a) Fractional power function kinetic model

| | $a$ | $b$ | $ab$ | $R^2$ |
|---|---|---|---|---|
| B.G. | 20.08 | 0.153 | 3.07 | 0.967 |
| C.V. | 21.97 | 0.148 | 3.25 | 0.977 |

(b) The pseudo-first-order kinetic (Lagergren) model

| | $q_{e,\exp}$ (mg/g) | $q_{e,\text{calc}}$ (mg/g) | $k_1$ | $R^2$ |
|---|---|---|---|---|
| B.G. | 38.77 | 21.68 | 0.046 | 0.969 |
| C.V. | 41.91 | 18.37 | 0.047 | 0.983 |

(c) The pseudo-second-order kinetic model

| | $q_{e,\exp}$ (mg/g) | $q_{e,\text{calc}}$ (mg/g) | $k_2$ | $R^2$ |
|---|---|---|---|---|
| B.G. | 38.77 | 40.16 | 5.17 x $10^{-3}$ | 0.995 |
| C.V. | 41.91 | 43.1 | 6.9 x $10^{-3}$ | 0.999 |

(d) Elovich kinetic model

| | $\alpha$ (g/mg·min) | $\beta$ (mg/g·min) | $R^2$ |
|---|---|---|---|
| B.G. | 15.227 | 4.375 | 0.945 |
| C.V. | 12.202 | 4.945 | 0.978 |

the time plot (Figure 14) was linear. The computed values of $q_e$ and $K_{\text{Lager}}$ for B.G. dye were 21.68 mg/g and 0.046 $\text{min}^{-1}$, respectively, wherein the correlation coefficient $R^2 = 0.969$. However, for C.V. dye, the values of $q_e$ and $K_{\text{Lager}}$ were 18.37 mg/g and 0.047 $\text{min}^{-1}$, respectively, whereby correlation coefficient $R^2 = 0.983$. Nonetheless, inconsistency has been observed between the derived results and the first-order kinetics of adsorption of B.G. and C.V. dye species on the binary P3NT/30%$AgTiO_2$ NCs [38].

The pseudo-second-order equation has further been outlined as a distinct variety of Langmuir kinetics [39], according to the following presumptions: (i) constant adsorbate concentration over time and (ii) determination of the amount of adsorbate at equilibrium with the aid of binding positions. The following equation expresses the linear form of the pseudo-second-order rate:

$$\frac{t}{qt} = \frac{1}{h} + \left(\frac{1}{qe}\right)t, \tag{5}$$

where $h = k_2 q_e{}^2$ explains the primary sorption rate adsorbed per unit mass at equilibrium, while $q_e$ and $q_t$ epitomize the rate of adsorption at various time intervals. Herein, $t/q_t$ versus $(t)$ plots were linear, as displayed in Figure 15. The slope-intercept $(k_2)$ and $(q_e)$ for (B.G.) species of dyes was calculated at $5.17 \times 10^{-3}$ g $(\text{mg·min})^{-1}$ and 40.16 mg/g, respectively, with perfect correlation $(R^2 = 0.996)$. On the other hand, the slope-intercept ($k_2$ and $q_e$) for species of C.V. dyes was determined as equal to $6.9 \times 10 - {}^3$ g $(\text{mg·min})^{-1}$ and 43.10 mg/g, respectively, with good correlation $(R^2 = 0.999)$. The data concludes a strong match between pseudo-second-order rate constant, $k_2$, and the empirical values that are mostly influenced by the experimental environment factors, including temperature, pH of the solution, and fundamental metal concentration [40].

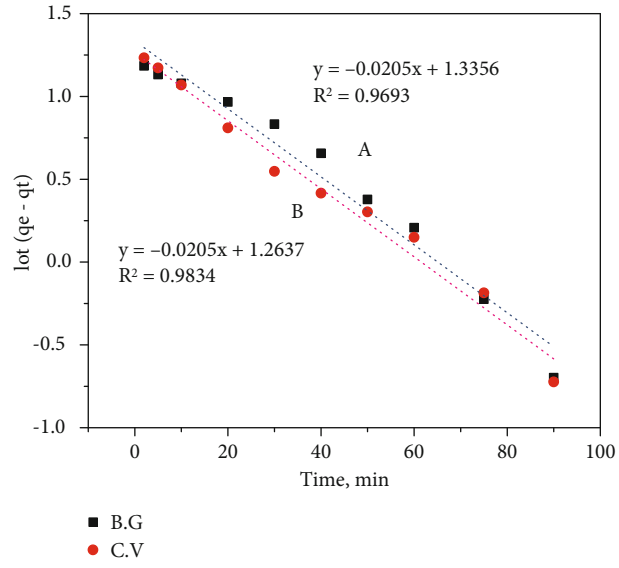


Figure 14: Lagergren plot of B.G. and C.V. dyes' adsorption onto the binary P3NT/30%$AgTiO_2$ NCs versus time. Experimental conditions are represented in the batch extraction step.

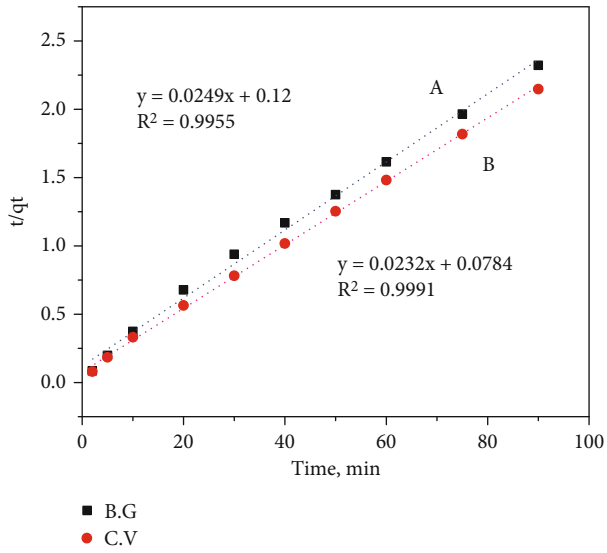


Figure 15: Pseudo-second-order depiction of B.G. and C.V. dyes' adsorption on the binary P3NT/30%AgTiO$_2$ NCs versus time. Experimental conditions are illustrated in the batch extraction step.

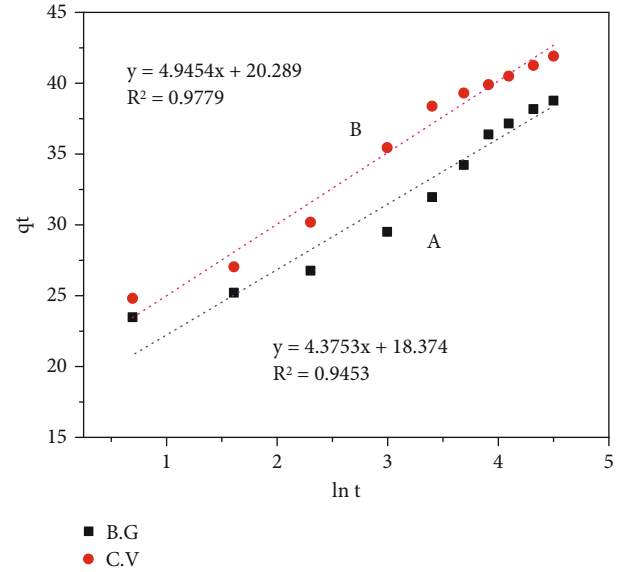


Figure 16: Elovich model graph for B.G. and C.V. dyes' uptake on the surface of binary P3NT/30%AgTiO$_2$ NCs versus time. Experimental conditions are illustrated in the batch extraction step.

The Elovich model is one of the significant equations representing adsorption potential [41]. Usually, it is used for studying the kinetics of chemisorption and heterogeneous absorbent surfaces. The below-mentioned equation can be engaged to illustrate this model:

$$q_t = \beta \ln(\alpha\beta) + \beta \ln t, \tag{6}$$

where $\beta$ (mg·g$^{-1}$·min$^{-1}$) is the coefficient of desorption and $\alpha$ (g·mg$^{-1}$·min$^{-1}$) stands for the initial adsorption rate. In this depiction, $q_t$ against ln $t$ plot was linear (Figure 16). The Elovich parameters, namely, $\beta$ and $\alpha$, computed from the slopes and the intercepts (Figure 16) for species of dyes were found equivalent to 15.227 g·mg$^{-1}$·min$^{-1}$ and 4.375 mg·g$^{-1}$·min$^{-1}$, respectively, with ($R^2 = 0.945$) for B.G. dye adsorbed onto the binary P3NT/30%AgTiO$_2$ NCs. Similarly, for C.V. dye adsorbed onto the binary P3NT/30%AgTiO$_2$ NCs, the corresponding values were found equal to 12.202 g·mg$^{-1}$·min$^{-1}$ and 4.945 mg.g$^{-1}$·min$^{-1}$, respectively, with ($R^2 = 0.978$).

The empirical data from the previous sections were further dealt with in the following kinetic models to fit the adsorption of dyes of B.G. and C.V. varieties: (I) function of fractional power, (II) Lagergren's pseudo-first order, (III) the pseudo-second order, and (IV) Elovich frameworks, as depicted in Table 2. The consequent correlation coefficient variables revealed that the kinetic pseudo-second-order model was the most appropriate kinetic model, which illustrates binary P3NT/30%AgTiO$_2$ NC dye adsorption from a liquid phase. Compared with previous studies (Table 3), the binary P3NT/30%AgTiO$_2$ NC in this study has a higher sorption capacity.

*3.5. Thermodynamics of B.G. and C.V. Dye Retention on the Surface of Binary P3NT/30%AgTiO$_2$ NCs.* The preservation of pigments on binary adsorbent P3NT/30%AgTiO$_2$ NCs and the adsorption rates of B.G. and C.V. dyes on the surface of binary P3NT/30%AgTiO$_2$ NC adsorbent need to be evaluated under a broad series of temperatures between 293 and 323 K. The thermodynamic criteria ($\Delta S$, $\Delta H$, and $\Delta G$) were estimated with the help of following equations [42]:

$$\begin{aligned} \ln K_c &= \frac{-\Delta H}{RT} + \frac{\Delta S}{R}, \\ \Delta G &= \Delta H - T\Delta S, \\ \Delta G &= -RT \ln K_c. \end{aligned} \tag{7}$$

$\Delta S$, $\Delta H$, and $\Delta G$ imply the entropy, enthalpy, and Gibbs-free energy changes, respectively. $R$ is the constant for the gaseous phase (≈8.314 J·K$^{-1}$·mol$^{-1}$), $T$ stands for temperature (unit-Kelvin), whereas $K_C$ is the equilibrium constant. Determination of the $K_C$ values for retention of B.G. and C.V. dyes from the experimental aqueous media on the solid sorbent surface at equilibrium was done by applying the following equation:

$$k_c = \frac{C_a}{C_e}. \tag{8}$$

The balancing concentration of the dye species (B.G. and C.V.) in an aqueous media (mg·L$^{-1}$) is expressed by $C_e$. The amount of B.G. and C.V. dyes that undergo adsorption at equilibrium (mg·L$^{-1}$) on the surface of per liter solid-phase sorbent is represented by $C_a$. The layout of ln $K_C$ against 1000/$T$ for retaining the B.G. and C.V. dyes on the binary P3NT/30%AgTiO$_2$ NCs under the temperature range of

Table 3: The comparison of $q_e$ with various adsorbents.

| Dyes | Adsorbents | $q_{e,\,calc}$ (mg·g$^{-1}$) | Ref. |
|---|---|---|---|
| B.G. | Binary P3NT/30%AgTiO$_2$ NCs | 40.16 | This work |
| | *Bambusa tulda* (NCBT) | 4.73 | [43] |
| | *Salix alba* leaves (SAL) | 15.87 | [44] |
| | Unmodified lemon peel waste | 31.31 | [45] |
| | Kaolinite clay minerals | 18.90 | [46] |
| C.V. | Binary P3NT/30%AgTiO$_2$ NCs | 43.1 | This work |
| | Kaolinite clay minerals | 33.78 | [46] |
| | Zinc oxide nanoparticle loaded on activated carbon (ZnO-NP-AC) | 13.11 | [47] |
| | Modified *Bambusa tulda* | 4.95 | [48] |
| | Olive leave powder (OLP) | 12.32 | [49] |

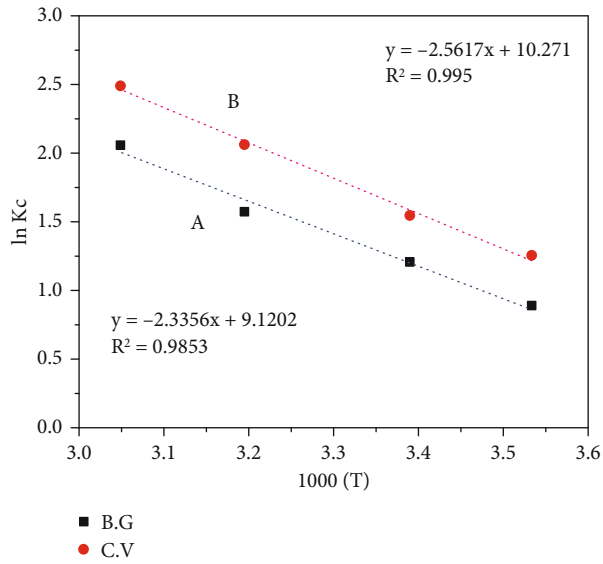


Figure 17: Graph of ln $K_C$ of B.G. and C.V. dyes' sorption from aqueous solutions to the binary P3NT/30%AgTiO$_2$ NCs versus 1000/$T$.

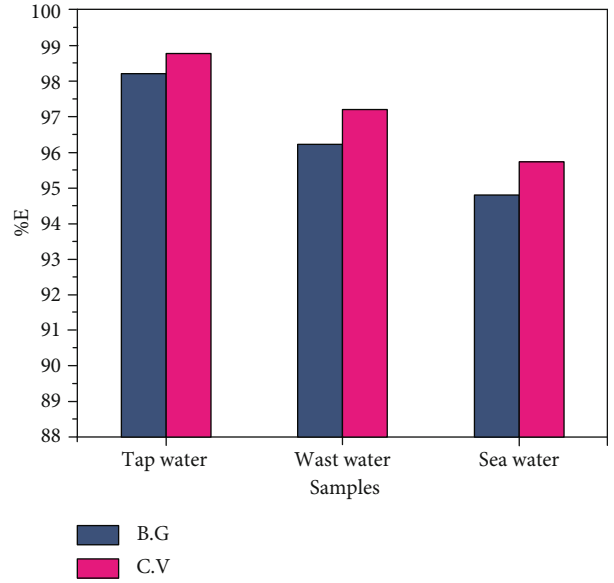


Figure 18: The removal efficiency of B.G. and C.V. dyes from multiple real samples of the binary P3NT/30%AgTiO$_2$ NC solid phase (experimental environment: 50 mL solution, B.G. concentration of 5 mg·L$^{-1}$, pH = 6, and 25 mg of binary P3NT/30%AgTiO$_2$ NCs for B.G. dye and 50 mL solution, pH = 8, C.V. concentration of 5 mg·L$^{-1}$, and 25 mg of the P3NT/30%AgTiO$_2$ NCs for C.V. dye and stirring time = 90 min and temperature = 295 K).

283–328 K was a linear graph (Figure 17). The balancing constant continues to increase with the rising temperature, confirming the endothermal retention process of B.G. and C.V. dyes on the binary adsorbent P3NT/30%AgTiO$_2$ NCs. The arithmetic values of $\Delta H$, $\Delta S$, and $\Delta G$ for retaining the dyes' species were derived from the slope and intersectional point of the linear depiction of ln $K_C$ versus 1000/$T$ (Figure 17), whose values were $19.37 \pm 0.12\,\mathrm{K \cdot J \cdot mol^{-1}}$, $75.82 \pm 0.34\,\mathrm{J \cdot mol^{-1} \cdot K^{-1}}$, and $-2.99 \pm 0.06\,\mathrm{K \cdot J \cdot mol^{-1}}$ (at 295 K), respectively, for B.G. dye. Likewise, the corresponding values derived for C.V. dyes were $21.28 \pm 0.24\,\mathrm{K \cdot J \cdot mo}$ $\mathrm{l^{-1}}$, $85.38 \pm 0.38\,\mathrm{J \cdot mol^{-1} \cdot K^{-1}}$, and $-3.91 \pm 0.08\,\mathrm{K \cdot J \cdot mol^{-1}}$ (at 295 K). The $\Delta H$ value derived from the study marks the process of endothermic adsorption, whereas the examination of the analyte and the sorbent value leads to differential bond power. A positive $\Delta S$ value of the binary P3NT/30%AgTiO$_2$ NCs highlights the increased flexibility at the boundaries of solid-liquid phases. This occurs when the hydrogen sphere loses $H_2O$ molecules, mostly due to the adsorption processes of the B.G. and C.V. dye species; the negative $\Delta G$ value alters the physical adsorption of binary P3NT/30%AgTiO$_2$ NC adsorbent at 295 K, thus reflecting spontaneously in B.G. and C.V. dyes' retention on binary P3NT/30%AgTiO$_2$ NCs.

*3.6. Environmental Applications.* The examination of authentic environmental specimens would assist in assessing the applicability of binary P3NT/30% AgTiO$_2$ NCs for estrogenic chemicals' removal. To fulfill this study's objective, three categories of water samples were gathered from varied sources, like (I) the Red Sea's water (the Red Sea in front of Jeddah city, KSA), (II) tap water from the chemistry laboratories of the University of Jeddah, Jeddah city, KSA, and (III)

sample of wastewater collected from processing plant located at King Abdulaziz University, Jeddah city, KSA. Examination of the samples enabled the measurement of dye concentration, revealing a lower identification limit as compared to UV-vis analysis. While processing the samples, a mix of 25 mg of binary P3NT/30%$AgTiO_2$ NCs and 5 mg·$L^{-1}$ of B.G. dye was poured into the solution and the pH was set to 6. Subsequently, the experimental solution was subjected to mechanical stirring at 295 K for a time of 90 minutes. Similarly, the removal efficiency of B.G. and C.V. dyes from the specimens has been illustrated in Figure 18. Four consecutive cycles of the processes, including collection, washing, and drying, followed by reutilization of the binary P3NT/30%$AgTiO_2$ NCs for B.G. and C.V. dyes' removal were conducted, and all of them yielded identical removal efficiency.

## 4. Conclusion

To summarize, the successful fabrication of the nanocomposites of binary poly(3-nitrothiophene)/silver titanium dioxide was performed through the in situ technique of polymerization by using variable quantities of $AgTiO_2$. Additionally, the batch adsorption method was engaged to assess their competence in eliminating hazardous B.G. and C.V. dyes. The FTIR and XRD manifest the binary NCs' creation. Likewise, the shadowing of $AgTiO_2$ NPs by the P3NT has been demonstrated by the outcomes of EDX and SEM tests. A substantial increase in the removal ability and power of adsorption of P3NT/30% $AgTiO_2$ NCs was demonstrated by the UV-vis spectroscopy's outcomes in contrast to pure P3NT as well other NCs. Moreover, according to the data, the pseudo-second-order model fits better than other thermodynamics with adsorption of B.G. and C.V. pigments on the walls of the adsorbent compound. In addition, the maximal adsorption capacity of 40.16 mg/g for B.G. dye and 43.10 mg/g for C.V. dye was shown by this adsorbent. The adsorption system, on the other hand, was endothermal, thereby following the kinetic framework of the pseudo-second-order model. Furthermore, P3NT/30%$AgTiO_2$ NCs have an excellent potential of removal, thus promoting their reuse post four cycles consecutively. Hence, due to their high efficiency and benefits in removing hazardous dyes, P3NT/30%$AgTiO_2$ NC adsorbents could be evaluated as likely environmental remedial adsorbents.

## Data Availability

No research data are not shared.

## Conflicts of Interest

The author declares that they have no conflicts of interest.

## Acknowledgments

This work was funded by the University of Jeddah, Jeddah, Saudi Arabia, under grant no. (UJ-21-DR-29). The authors, therefore, acknowledge with thanks the University of Jeddah technical and financial support.

## Supplementary Materials

Figure S1: $^1$H-NMR spectrum of P3NT. *(Supplementary Materials)*

## References

[1] B. Ismail, S. T. Hussain, and S. Akram, "Adsorption of methylene blue onto spinel magnesium aluminate nanoparticles: adsorption isotherms, kinetic and thermodynamic studies," *Chemical Engineering Journal*, vol. 219, pp. 395–402, 2013.

[2] Y. Xie, C. He, L. Liu et al., "Carbon nanotube based polymer nanocomposites: biomimic preparation and organic dye adsorption applications," *RSC Advances*, vol. 5, no. 100, pp. 82503–82512, 2015.

[3] R. H. Althomali, K. A. Alamry, M. A. Hussein, A. Khan, S. S. Al-Juaid, and A. M. Asiri, "Modification of alginic acid for the removal of dyes from aqueous solutions by solid-phase extraction," *International Journal of Environmental Analytical Chemistry*, pp. 1–21, 2020.

[4] A. Salama, K. R. Shoueir, and H. A. Aljohani, "Preparation of sustainable nanocomposite as new adsorbent for dyes removal," *Fibers and Polymers*, vol. 18, no. 9, pp. 1825–1830, 2017.

[5] K. Y. Foo and B. H. Hameed, "Preparation, characterization and evaluation of adsorptive properties of orange peel based activated carbon via microwave induced K2CO3 activation," *Bioresource Technology*, vol. 104, pp. 679–686, 2012.

[6] L. Prola, E. Acayanka, E. Lima et al., "Comparison of Jatropha curcas shells in natural form and treated by non-thermal plasma as biosorbents for removal of reactive red 120 textile dye from aqueous solution," *Industrial Crops and Products*, vol. 46, pp. 328–340, 2013.

[7] N. Kataria and V. K. Garg, *Application of EDTA Modified Fe3O4/Sawdust Carbon Nanocomposites to Ameliorate Methylene Blue and Brilliant Green Dye Laden Water, Vol. 172*, Elsevier Inc., 2019.

[8] E. Makhado, S. Pandey, P. N. Nomngongo, and J. Ramontja, "Preparation and characterization of xanthan gum-cl-poly(-acrylic acid)/o-MWCNTs hydrogel nanocomposite as highly effective re-usable adsorbent for removal of methylene blue from aqueous solutions," *Journal of Colloid and Interface Science*, vol. 513, pp. 700–714, 2018.

[9] G. Vyavahare, P. Jadhav, J. Jadhav et al., "Strategies for crystal violet dye sorption on biochar derived from mango leaves and evaluation of residual dye toxicity," *Journal of Cleaner Production*, vol. 207, pp. 296–305, 2019.

[10] A. C. Bhasikuttan, A. V. Sapre, and L. V. Shastri, "Photoinduced electron transfer in crystal violet (CV+)-bovine serum albumin (BSA) system: evaluation of reaction paths and radical intermediates," *Journal of Photochemistry and Photobiology A: Chemistry*, vol. 150, no. 1–3, pp. 59–66, 2002.

[11] H. Mittal, S. M. Alhassan, and S. S. Ray, "Efficient organic dye removal from wastewater by magnetic carbonaceous adsorbent prepared from corn starch," *Journal of Environmental Chemical Engineering*, vol. 6, no. 6, pp. 7119–7131, 2018.

[12] M. Elkady, H. Shokry, A. El-Sharkawy, G. El-Subruiti, and H. Hamad, "New insights into the activity of green supported nanoscale zero-valent iron composites for enhanced acid blue-

25 dye synergistic decolorization from aqueous medium," *Journal of Molecular Liquids*, vol. 294, 2019.

[13] A. S. Eltaweil, H. Ali Mohamed, E. M. Abd El-Monaem, and G. M. El-Subruiti, "Mesoporous magnetic biochar composite for enhanced adsorption of malachite green dye: characterization, adsorption kinetics, thermodynamics and isotherms," *Advanced Powder Technology*, vol. 31, no. 3, pp. 1253–1263, 2020.

[14] A. S. Eltaweil, G. S. Elgarhy, G. M. El-Subruiti, and A. M. Omer, "Carboxymethyl cellulose/carboxylated graphene oxide composite microbeads for efficient adsorption of cationic methylene blue dye," *International Journal of Biological Macromolecules*, vol. 154, pp. 307–318, 2020.

[15] R. Rehman, T. Mahmud, and M. Irum, "Brilliant green dye elimination from water using Psidium guajava leaves and Solanum tuberosum peels as adsorbents in environmentally benign way," *Journal of Chemistry*, vol. 2015, Article ID 126036, 8 pages, 2015.

[16] S. M. Mousavi, A. Babapoor, S. A. Hashemi, and B. C. Medi, "Adsorption and removal characterization of nitrobenzene by graphene oxide coated by polythiophene nanoparticles," *Physical Chemistry Research*, vol. 8, no. 2, pp. 225–240, 2020.

[17] A. Majumder and A. K. Gupta, "Enhanced photocatalytic degradation of 17$\beta$-estradiol by polythiophene modified Al-doped ZnO: optimization of synthesis parameters using multivariate optimization techniques," *Journal of Environmental Chemical Engineering*, vol. 8, no. 6, article 104463, 2020.

[18] A. Majumdar and A. Pal, "Optimized synthesis of Bi4NbO8Cl perovskite nanosheets for enhanced visible light assisted photocatalytic degradation of tetracycline antibiotics," *Journal of Environmental Chemical Engineering*, vol. 8, no. 1, article 103645, 2020.

[19] R. Shan, L. Lu, J. Gu et al., "Photocatalytic degradation of methyl orange by Ag/TiO2/biochar composite catalysts in aqueous solutions," *Materials Science in Semiconductor Processing*, vol. 114, article 105088, 2020.

[20] A. C. Mecha, M. S. Onyango, A. Ochieng, and M. N. B. Momba, "Evaluation of synergy and bacterial regrowth in photocatalytic ozonation disinfection of municipal wastewater," *Science of the Total Environment*, vol. 601-602, pp. 626–635, 2017.

[21] T. D. Pham and B. K. Lee, "Effects of Ag doping on the photocatalytic disinfection of E. coli in bioaerosol by Ag-TiO2/GF under visible light," *Journal of Colloid and Interface Science*, vol. 428, pp. 24–31, 2014.

[22] O. Nasr, O. Mohamed, A. S. Al-Shirbini, and A. M. Abdel-Wahab, "Photocatalytic degradation of acetaminophen over Ag, Au and Pt loaded TiO 2 using solar light," *Journal of Photochemistry and Photobiology A: Chemistry*, vol. 374, pp. 185–193, 2019.

[23] E. A. Abdullah, A. H. Abdullah, and Z. Zainal, "TiO2/Ag modified penta-bismuth hepta-oxide nitrate and its adsorption performance for azo dye removal," *Journal of Environmental Sciences*, vol. 24, no. 10, pp. 1876–1884, 2012.

[24] A. Blatp, S. Bach, and L. Kresc, "2-Nitro-, 3-nitro-, 2, 4-dinitro-, and 2, 5-dinitrothiophene 1," *The Journal of Organic Chemistry*, vol. II, pp. 1693–1695, 1957.

[25] M. O. Ansari, M. M. Khan, S. A. Ansari, J. Lee, and M. H. Cho, "Enhanced thermoelectric behaviour and visible light activity of Ag@TiO 2/polyaniline nanocomposite synthesized by biogenic-chemical route," *RSC Advances*, vol. 4, no. 45, pp. 23713–23719, 2014.

[26] M. Khatamian, M. Fazayeli, and B. Divband, "Preparation, characterization and photocatalytic properties of polythiophene-sensitized zinc oxide hybrid nanocomposites," *Materials Science in Semiconductor Processing*, vol. 26, no. 1, pp. 540–547, 2014.

[27] B. Senthilkumar, P. Thenamirtham, and R. Kalai Selvan, "Structural and electrochemical properties of polythiophene," *Applied Surface Science*, vol. 257, no. 21, pp. 9063–9067, 2011.

[28] S. Murugavel and M. Malathi, "Structural, photoconductivity, and dielectric studies of polythiophene-tin oxide nanocomposites," *Materials Research Bulletin*, vol. 81, pp. 93–100, 2016.

[29] F. Kong, Y. Wang, J. Zhang et al., "The preparation and gas sensitivity study of polythiophene/SnO2 composites," *Science & Engineering B: Solid-State Materials for Advanced Technology*, vol. 150, no. 1, pp. 6–11, 2008.

[30] R. D. Kross and V. A. Fassel, "The infrared spectra of aromatic compounds. IV. The nitro valence vibrations in p-disubstituted nitrobenzenes1," *Journal of the American Chemical Society*, vol. 78, no. 17, pp. 4225–4229, 1956.

[31] M. Liu, J. Zhao, C. Xiao, Q. Quan, and X. Li, "PPy-assisted fabrication of Ag/TiO2 visible-light photocatalyst and its immobilization on PAN fiber," *Materials and Design*, vol. 104, pp. 428–435, 2016.

[32] A. Husain, S. Ahmad, and F. Mohammad, "Thermally stable and highly sensitive ethene gas sensor based on polythiophene/zirconium oxide nanocomposites," *Materials Today Communications*, vol. 20, article 100574, 2019.

[33] K. Jyoti, M. Baunthiyal, and A. Singh, "Characterization of silver nanoparticles synthesized usingUrtica dioicaLinn. leaves and their synergistic effects with antibiotics," *Journal of Radiation Research and Applied Science*, vol. 9, no. 3, pp. 217–227, 2016.

[34] S. Sambaza, A. Maity, and K. Pillay, "Enhanced degradation of BPA in water by PANI supported Ag/TiO2 nanocomposite under UV and visible light," *Journal of Environmental Chemical Engineering*, vol. 7, no. 1, 2019.

[35] S. Dastgheib and D. Rockstraw, "A systematic study and proposed model of the adsorption of binary metal ion solutes in aqueous solution onto activated carbon produced from pecan shells," *Carbon N. Y.*, vol. 40, no. 11, pp. 1853–1861, 2002.

[36] R. C. Dalal, "Desorption of soil phosphate by anion-exchange resin," *Communications in Soil Science and Plant Analysis*, vol. 5, no. 6, pp. 531–538, 1974.

[37] A. Bhattacharya and C. Venkobachar, "Removal of cadmium (II) by low cost adsorbents," *Journal of Environmental Engineering*, vol. 110, no. 1, pp. 110–122, 1984.

[38] M. El-Shahawi, M. Othman, and M. Abdel-Fadeel, "Kinetics, thermodynamic and chromatographic behaviour of the uranyl ions sorption from aqueous thiocyanate media onto polyurethane foams," *Analytica Chimica Acta*, vol. 546, no. 2, pp. 221–228, 2005.

[39] H. M. Al-Saidi, M. A. Abdel-Fadeel, A. Z. El-Sonbati, and A. A. El-Bindary, "Multi-walled carbon nanotubes as an adsorbent material for the solid phase extraction of bismuth from aqueous media: kinetic and thermodynamic studies and analytical applications," *Journal of Molecular Liquids*, vol. 216, pp. 693–698, 2016.

[40] L. Heights and O. Ridge, "Some development for radioanalytical separations," *Journal of Radioanalytical and Nuclear Chemistry*, vol. 84, no. 2, pp. 461–472, 1984.

[41] M. A. Salam and R. M. Mohamed, "Removal of antimony (III) by multi-walled carbon nanotubes from model solution and environmental samples," *Chemical Engineering Research and Design*, vol. 91, no. 7, pp. 1352–1360, 2013.

[42] S. A. Hameed, M. A. Abdel-Fadeel, H. M. Al-Saidi, and M. A. Salam, "Simultaneous removal of the toxic tungsten ions and rhodamine B dye by graphene nanosheets from model and real water," *Desalination and Water Treatment*, vol. 188, pp. 266–276, 2020.

[43] N. Laskar and U. Kumar, "Removal of brilliant green dye from water by modified Bambusa tulda: adsorption isotherm, kinetics and thermodynamics study," *International journal of Environmental Science and Technology*, vol. 16, no. 3, pp. 1649–1662, 2019.

[44] R. Fiaz, M. Hafeez, and R. Mahmood, "Removal of brilliant green (BG) from aqueous solution by using low cost biomass Salix alba leaves (SAL): thermodynamic and kinetic studies," *Journal of Water Reuse and Desalination*, vol. 10, no. 1, pp. 70–81, 2020.

[45] A. Aichour and H. Zaghouane-Boudiaf, "Highly brilliant green removal from wastewater by mesoporous adsorbents: kinetics, thermodynamics and equilibrium isotherm studies," *Microchemical Journal*, vol. 146, pp. 1255–1262, 2019.

[46] A. A. Romzi, M. R. R. Kooh, L. B. L. Lim, N. Priyantha, and C. M. Chan, "Environmentally friendly adsorbent derived from rock melon skin for effective removal of toxic brilliant green dye: linear versus non-linear analyses," *International Journal of Environmental Analytical Chemistry*, pp. 1–20, 2021.

[47] R. Karimi, F. Yousefi, M. Ghaedi, and Z. Rezaee, "Comparison the behavior of ZnO–NP–AC and Na, K doped ZnO–NP–AC for simultaneous removal of crystal violet and quinoline yellow dyes: modeling and optimization," *Polyhedron*, vol. 170, pp. 60–69, 2019.

[48] N. Laskar and U. Kumar, "Adsorption of crystal violet from wastewater by modified Bambusa tulda," *KSCE Journal of Civil Engineering*, vol. 22, no. 8, pp. 2755–2763, 2018.

[49] K. M. Elsherif, A. El-Dali, A. A. Alkarewi, A. M. Ewlad-ahmed, and A. Treban, "Adsorption of crystal violet dye onto olive leaves powder: equilibrium and kinetic studies," *Chemistry International*, vol. 7, no. 2, pp. 79–89, 2021.